Superhydrophobic Electrospun Membrane for Heavy Metals Removal by Air Gap Membrane Distillation (AGMD)

Hadi Attia [a], Shirin Alexander[b], Chris J. Wright [c], Nidal Hilal [a*]

[a] Centre for Water Advanced Technologies and Environmental Research (CWATER), College of Engineering, Swansea University, Fabian Way, Swansea SA1 8EN, UK.

[b] Energy Safety Research Institute (ESRI), Swansea University, Swansea SA1 8EN, UK.

[c] Biomaterials, Biofouling and Biofilms Engineering Laboratory (B^3EL), The Systems and Process Engineering Centre (SPEC), College of Engineering, Swansea University, Swansea SA1 8EN, UK.

*Corresponding author: n.hilal@swansea.ac.uk

Abstract

This paper presents a novel approach to fabricate superhydrophobic membranes by using environmentally friendly and cost effective superhydrophobic nanoparticles to enhance nanofibrous membrane performance in term of flux and rejection of heavy metals in Membrane distillation applications. Polyvinylidene fluoride (PVDF) membranes were fabricated using an electrospinning technique, in which electrospinning parameters such as polymer concentration, voltage, solvent ratio, and cationic surfactant were studied to optimize the membrane fibre diameters and produce beadless nanofibrous membranes. The nanofibrous membranes were characterized in terms of pore size, porosity, liquid entry pressure, contact angle, permeate flux and rejection percentage, and were compared to a commercial membrane. Air gap membrane distillation (AGMD) was used to demonstrate the improved ability of superhydrophobic PVDF membranes for removing heavy metals (such as lead) in comparison with pristine and commercial membranes. The results showed that pristine beadless membrane mat can be fabricated by using 15 wt% polymer concentration, 0.05 wt% cationic surfactant with 6:4 DMF to acetone ratio and 14 KV with lead rejection rate of 72.77 %, liquid entry pressure (17 psi) and water contact angle of 132º. In comparison, the composite 11 wt% PVDF membranes with 20 wt% of functionalized alumina (Al_2O_3) showed 150º WCA and 27 psi as liquid entry pressure which led to 99.36 % of heavy metal rejection and 5.9% increase in permeate flux.

Keywords

superhydrophobic membrane, electrospinning, membrane distillation, surfactant, heavy metals, superhydrophobic nanoparticles.

1. Introduction

One of the main challenges of the current era is water shortage and environmental pollution issues with the natural water. Additionally, Industrial activities, population growth, development of the agricultural sector as well as urbanization have exacerbated the problem [1]. Therefore, desalination of salt water and reusing polluted water must be considered. In the case of reusing polluted water from chemical industries, efficient and effective methods are required. One of the biggest problems concerning environmental pollution is the existence of heavy metals in some industrial effluent and wastewater. For instant, arsenic, mercury, lead, chromium, cadmium, copper, silver, nickel and zinc are the most common toxic heavy metals with non-biodegradable nature in wastewater [2]. The main sources of these heavy metals are industrial activities such as mining, printed circuit board manufacturing, wood processing industry, electroplating, pulp and paper, printing, petrochemicals, phosphate fertilizer, steel industries, battery industry and many more [3, 4]. Heavy metals can cause significant environmental and health problems such as depressing the growth of living organisms and cancer and damage to the human nervous system respectively. They are considered to be toxic to the human being due to bioaccumulation owing to inability to be metabolized and by the digestion system. Exposure to some metal, such as lead, might also results in extra problems in children such as learning disabilities, growth problem and anti-social behaviour [2].According to Environmental Protection Agency (EPA) the maximum lead (Pb) concentration allowed in the wastewater discharge is 0.05 mg/l [5].

Many methods have been employed to remove heavy metals from wastewater such as adsorption, chemical precipitation and electrochemical removal [6, 7]. However, these techniques suffer some disadvantages, such as inadequate removal rate and high energy demand [8]. On the other hand, elimination of heavy metals by membrane technology are highly recommended due to the high rejection rate of heavy metals especially in low concentration [9].

Ultrafiltration permeable membranes can be harnessed to reject dissolved and colloidal material which has a particle size larger than the membrane pore size (5–20 nm) as well as separating compounds with a molecular weight of 1000– 100,000 Da [9]. This can be achieved

by increasing the particle size of metal ions using various methods such as polymer enhanced ultrafiltration (PEUF) and micellar enhanced ultrafiltration (MEUF) [7]. PEUF is based on creating a macromolecular complex of metallic ions by mixing wastewater polluted with heavy metals and a water-soluble polymer which has a molecular weight higher than the membrane's molecular weight cut-off. On the other hand, the MEUF method can be achieved by adding a surfactant (above its critical micelle concentration, cmc) to wastewater which causes an increase in particle size of metal ions by the binding of metal ions around micelles, resulting in large metal-surfactant structures. However, the main disadvantages of these methods are the insufficient removal of heavy metals (around 90%) and limited threshold of heavy metals concentration in the feed line, such as 112 mg/l [6].

Beside the ultrafiltration techniques, nanofiltration (NF) can be used to retain metal ions larger than 1nm [10]. The advantages of employing NF compared to reverse osmosis (RO) which is a semi-permeable membrane to remove a wide range of dissolved species from wastewater are low energy consumption and that it can be used with lower pressure [8]. However, the main disadvantage of NF is that a limitation of threshold of heavy metals concentration in the feed side can be fed due to membrane fouling obstacle as well as high membrane cost [11]. On the other hand, the main drawback of RO is the high pressure which needs to be employed, leading to high power consumption and a high capital cost to install the system [11, 12].

Hence, none of the above membrane techniques might be sufficient when the feed stream has a high concentration of metals. Membrane distillation (MD) which is a non-isothermal process can be found in different configurations such as direct contact membrane distillation (DCMD), air gap membrane distillation (AGMD), vacuum membrane distillation (VMD) and sweep gas membrane distillation, which offer a unique solution to overcome these problems. Generally, MD uses a porous and hydrophobic membrane that can be applied between the hot feed and cold permeate stream to achieve the separation process. This allows only vapour molecules to travel through the membrane depending on the trans-membrane vapour pressure difference across the membrane [13]. The most important benefit of AGMD compared with DCMD is to reduce the conduction heat flux loss from the membrane of the condensing surface due to introducing air gap between the membrane and condensate side. Also it is more cost effective compared with MD and VMD due to using an internal condenser [14, 15]. MD has been successfully used for removing non-volatile solutes dissolved fully in water and for wastewater treatment [16]. Another advantage of membrane distillation is that the operational temperature is lower than that of the distillation process and less operating pressure can be used compared

to pressure driven membranes such as NF and RO [17]. Thus, the capital and operation cost can be reduced significantly. Also, MD can be used in combination with other membrane technology such as NF and RO to increase the rejection rate of heavy metals.

Table 1 shows the research that has been carried out so far using MD applications in removing heavy metals in wastewater streams. Three different applications of MD have been used: DCMD, AGMD and VMD. The first research on using MD for tackling waste water with heavy metals was reported in 1997 [18]. The test was conducted by using DCMD and AGMD with a commercial membrane and used nickel as a heavy metals model. The authors used low Ni concentration (2.93 mg/l) for DCMD and moderate concentration (14.67 to 88 mg/l) for AGMD. Also, as can be seen in Table 1, the commercial membrane was used to remove arsenic and boron by using DCMD [19-21]. Recently, electrospun membrane made from PVDF combined with TiO_2 nanoparticles (NPs) was reported to remove six heavy metals (Co (II), Zn (II), Cu (II), Ni (II), Cd (II) and Pb (II)) with concentration between 10- 100 ppm using VMD technique [22]. Nonetheless, the membrane suffered from wetting in high vacuum pressure and the permeate flux was around 10 $l/m^2.h$ (LMH) for the feed water at 60 ºC and water contact angle (WCA) of 145 º.

Many attempts have been made to increase the electrospun membrane hydrophobicity made from PVDF, PVDF-PTFE, PES and so on to overcome membrane wettability and increase permeate flux. Different functionalized nanoparticles have been used such as SiO_2, TiO_2, Carbon nanotube (CNT) and clay to increase membrane roughness and reduce membrane wettability [23-26]. The main functionality of the NPs is silane and fluorinated groups as it shown in Table 2 which results in high water contact angles. However, these groups are very expensive and have environmental consequences [27]. It was shown recently that it is possible to achieve superhydrophobic surfaces using Al_2O_3 nanoparticles functionalized with highly branched hydrocarbons [28, 29]. In this study we present, for the first time, new approach of using these low surface energy NPs to improve the hydrophobicity of the membranes. HTAB surfactant was also used to reduce electrospun fibre diameter and enhance NPs dispersion in PVDF polymer solution. Additionally, we report for the first time, the removal of high concentration of heavy metal lead (Pb) using AGMD application.

Table 1 removal of heavy metals by MD application

Membrane	Heavy metal use	rejection	Reference

MD type	properties						MD parameters		Flux, Kg/m^2.h	
	type	Pore size, µm	Thickness, µm	Porosity, %	Name	Concentration, mg/L				
DCMD	Commercial, Vladipor	0.2	120	70	Ni	2.93	Feed temp= 40-60ºC. Cooling line= 15ºC. Flow rate= 1.08 L/m.	------	4-14.4	[18]
AGMD	Commercial, Vladipor	0.2	120	70	Ni	14.67-88	Feed temp= 60ºC. Cooling line= 20ºC. Flow rate= 1.25 L/m.	-------	6.5-4.3	[18]
AGMD	PTFE	0.2	?	80	As	0.24	Feed temp= 85ºC. Cooling line= 295ºC.	99.8		[19]
FO-MD	Commercial, hollow fiber (PP), Enka Microdyn	0.2	----		As	0.339 - 1.2	Feed temp= 25-34ºC. Cooling line= 20ºC. Flow rate= 1.6-4.16 L/m.	----	0.54	[20]
DCMD	self-made PVDF	0.15		80	As	40 - 2000		99.9	20.9	[30]
DCMD	Commercial, PTFE -PP, Membrane Solutions	0.2	150 - 175	0.35 - 80	As	1.2	Feed temp= 30-61ºC. Cooling line= 12 - 42ºC.	100	49.80	[21]
DCMD	Commercial, GVHP, Millipore	0.22	125	62	F	0 -200	Feed temp= 35-371ºC. Cooling line= 20ºC. Feed flow rate= 2.74 L/m.	99	8.57	[31]
VDMD	self-made ES -PVDF + TiO_2	0.32		72	Co, Zn, Cu, Ni, Cd, Pb	10 - 100	Feed temp= 65ºC. Cooling line= 20ºC. Feed flow rate= 2.74 L/m.			[22]

Table 2 NPs type with various functional group used to modify the surface energy.

Polymer	Nanoparticles	Function group	WCA, º	Reference

PVDF-HFP	TiO_2	1H, 1H, 2H,2H perfluorooctyltriethoxysilane (FTES)	153.4	[26]
PVDF	SiO_2	Octadecyltrichlorosilane (OTS) (CH3(CH2)16CH2SiCl3	160	[25]
Cellulose acetate	TiO_2	fluoroalkylsilane (FAS) CF3(CF2)7(CH2)2Si(OCH3)3	162	[32]
PVDF	SiO_2	Tetraethoxysilane (TEOS)	150	[33]

2. Materials and methods

2.1. Materials

Polyvinylidene fluoride pellets (Mw = 275000), Alumina NPs (Mw = 101.96, particle size = 13 nm), Acetone (Ac), Dimethylformamide (DMF), ethanol, isopropanol, and cationic surfactant hexadecyl trimethyl ammonium bromide (HTAB) were supplied by Sigma-Aldrich and used without purification. Isostearyl acids were provided by Nissan Chemical Industries. Lead (II) nitrate was purchased from fisher. Commercial PVDF membrane (HVHP29325, 0.22 µm diameter) obtained from Millipore.

2.2. Nanoparticles functionalization

In order to obtain superhydrophobic surfaces as well as reducing alumina NPs agglomeration in the PVDF dope solution, the hydrophilic alumina NPs were functionalized using Isostearyl acids as was shown previously by Alexander et al [28]. The functionalization process was achieved by dispersing 20 g of pristine alumina NPs in 250 ml of toluene and 77.82 g of Isostearyl acids before refluxing overnight. Then the functionalized Al_2O_3 NPs were purified by following steps: Firstly, the Al_2O_3 NPs solution was centrifuged for 30 min. Then it was washed twice with 30 ml isopropanol and once with 30 ml of ethanol followed by removing the solvent and unreacted carboxylic acid by using a centrifuge. Finally, Al_2O_3 NPs were dried overnight at 80 ºC and stored in plastic sealed containers until further use. The functionalized and unfunctionalized NPs were characterized previously by Alexander groups [28] in which SEM, FTIR and contact angle and the data are given in the Supporting Information.

2.3. Preparation of electrospinning solution

The polymer solution was prepared by dissolving various amounts of PVDF pellets (11 to 20 wt%) with or without different additives such as surfactant (0 to 0.5 wt%) and Al_2O_3 NPs (5 to 30 wt%) based on polymer weight in an optimized solvent mixture ratio of DMF to acetone (6:4). In the case of using Al_2O_3 NPs with PVDF polymer, the specific amount of HTAB surfactant was sonicated in the solvent mixture for 5 minutes followed by adding Al_2O_3 NPs and using further sonication for 30 minutes before adding the PVDF pellets. An incubator shaker was used at temperature of 50 ºC and speed of 200 rpm to prepare the spinning polymer solution. After 12 hours of shaking, the polymer solution was allowed to cool down to room temperature and then it was placed in a vacuum oven at room temperature to remove any excess acetone and preventing bubbles formation in the electrospinning tube between the syringe and the needle.

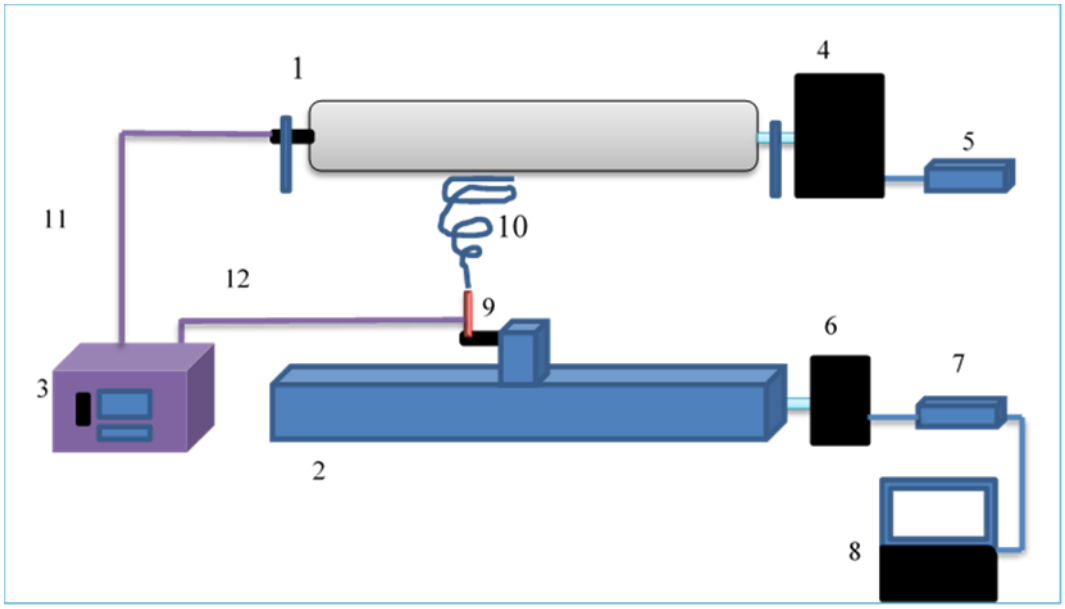

Figure 1: Schematic diagram of the drum Electrospinning device used in this study (1) Aluminium drum, (2) Actuator, (3) HV power supply, (4) Brushless motor, (5) Driver, (6) Stepper motor, (7) Driver, (8) Computer, (9) Needle, (10) Nano fiber, (11) Earth wire, (12) HV wire.

2.4. Electrospinning of membrane

Figure 1 shows homemade electrospinning apparatus used in this study which is consisted of six main components: an aluminium drum with a 100 mm in dimeter and 300 mm in length, connected to a DC brushless motor (BL300-H04-I, Applied motion, USA), a variable high positive voltage power supply (73030, Genvolt, UK), a syringe pump (cole-Parmer, USA), an

actuator with stepper motor (NEMA 17, Leadshine, USA) controlled by a computer via a driver (DM422, Leadshine, USA), a stainless steel needle (G 18) and a recording camera (1.3 MP, Chameleon). The electrospinning process was involved adjusting the speed of the grounded aluminium drum covered by aluminium foil to 500 rpm followed by setting the actuator speed to 8 cm/min. Then, the polymer solution is pumped via a syringe pump with flow rate between 0.1 to 0.6 ml/h to the stainless-steel needle through PTFE tube. The high voltage between 10 to 18 KV can be applied with the distance of 150 mm between the needle tip and the aluminium drum collector. In order to remove a residual solvent, membrane mats were heated for 3 h at 35 ° C.

2.5. Post treatment of PVDF membranes by hot-pressing method

Neat Electrospun membrane suffered from delamination layers and lack of mechanical strengths due to weak fibre connections. Therefore, heat-press post treatment was needed to upgrade membrane coherence and mechanical properties. Membrane heat press was conducted by applying pressure (6.27 kpa) at temperature 160 ºC for one hour. The process started by placing dry PVDF electrospun membrane, covered with aluminium foil on both sides, between two preheated flat metal plates with dimension of 150 × 100 mm and it was loaded with 4.79 kg as a dead weigh before it was placed in an oven.

2.6. Electrospun membrane characterization

2.6.1. Liquid entry pressure (LEP)

Liquid entry pressure (LEP) which is one of the main tests in MD applications was used to evaluate membrane wettability. LEP which is utilized to provide gaudiness for operating a pressure limit in membrane distillation can be conducted by measuring the pressure of deionizing water (DI) which is needed to overcome the membrane hydrophobicity. LEP, in this study, was engineered by using a home-made set-up which is consisted of an Amicon cell (50 ml) from Millipore with an effective surface area 13.4 cm^2 connected with pressurised nitrogen bottle through a pressure regulator and digital pressure gauge as it shown in Figure 2. LEP was measured by placing a dry membrane in Amicon cell followed by pressurizing the feed side of the membrane cell (full with 40 ml of distilled water) with nitrogen gas. The pressure was gradually increased by 1 psi every 10 mints started from 10 psi. The pressure value at which the first drop of DI water leaves the permeate side of the Amicon cell is called LEP. The test was repeated three times for all membranes.

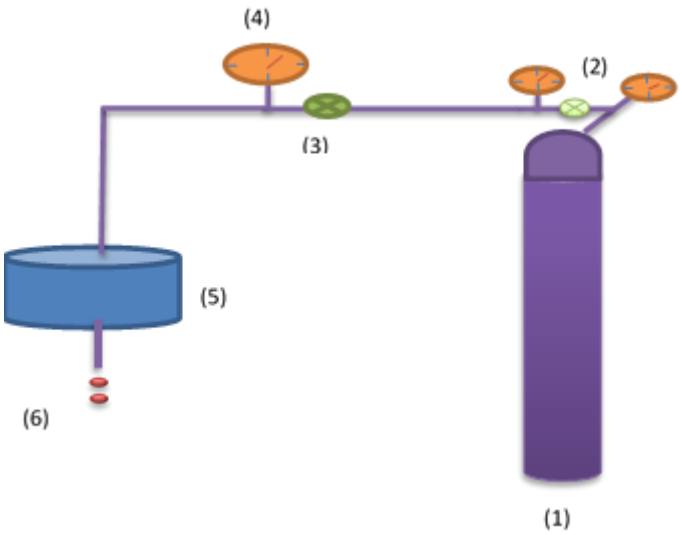

Figure 2: Schematic diagram of the home-made LEP apparatus, (1) Nitrogen gas cylinder, (2) Pressure regulator, (3) Regulator valve, (4) Pressure gauge, (5) Membrane cell, (6) Water droplets.

2.6.2. Water Contact angle (WCA)

The electrospun membrane hydrophobicity was evaluated by measuring the contact angle of membrane surface after conducting the electrospinning process. The water contact angle (WCA) was performed by using Expert Drop Shape Analyzer (Krüss model DSA25). The test was achieved by dropping 2 µl of DI water (using an automatic micro syringe) on a levelled dry membrane surface fixed on a glass slide by a double sided sticky tape. The contact angle was measured by using the sessile drop method with the help of a drop shape analysis program. The averages of five readings on different membrane spot were adopted with standard deviation less than 5.

2.6.3. Pore size and pore size distribution

Membrane pore sizes and pore size distributions were evaluated by using the bubble-point method. The custom-made device, shown in Figure 3, was employed to measure mean, maximum and minimum pore size. Isopropanol solvent with surface tension of 21.4 dynes/cm was used as a wetting liquid for dry ES membrane which was placed in Amicon membrane cell with an effective surface area of 13.4 cm^2. The test was performed by gradually increasing the nitrogen gas pressure on the feed side of the wet and dry nanofibrous membranes. The gas flow rate on the permeate side was recorded by using a gas and bubble flowmeter. The mean, maximum and minimum pore size values were computed from dry, half dry and wet curves which was drawn between flow rate and inlet pressure [17]. Firstly, both dry and half dry curves were measured without adding Isopropanol whereas wet curve is based on saturated of the

membrane with the solvent. The pressure value of cross point between wet curve and half dry curve represent the pressure of mean pore size, whereas the pressure at which wet curve meet dry curve is the pressure of minimum pore size. In addition, the lowest pressure which gives continuous gas flow was used to measure membrane maximum pore size. Equation 1 which represents the Young–Laplace Equation was used to calculate membrane pore size based on the corresponding pressure.

$$r = \frac{2y}{\Delta p} \times \cos\theta \qquad (1)$$

Where r is pore radius (µm), P is pressure difference (Pa) , y is isopropanol surface tension (mN/m)and Θ is membrane wetting angle (for completely wetted membrane by the fluid, cos Θ = 1).

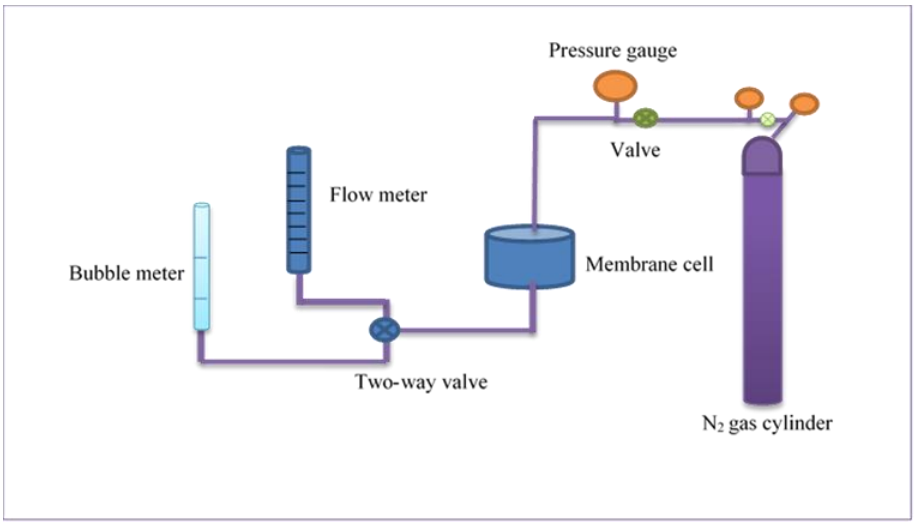

Figure 3: Schematic lay-out of the bubble point test.

2.6.4. Porosity measurement

Membrane porosity was adopted by using a gravimetric method which can be defined as the total volume of membrane pores divided by membrane volume [34]. The test was carried out by cutting a membrane area (2 cm × 2 cm) followed by weighting the membrane before and after immersing into an isopropanol solution for 10 minutes. Equation 2 has been employed for calculation of PVDF membrane porosity.

$$\rho = \frac{(W_1 - W_2) \times de}{[(W_1 - W_2)/de] + \frac{W_2}{dp}} \qquad (2)$$

Where ρ is the membrane porosity, W_1 is saturated membrane with isopropanol weight in gram, W_2 is the dry membrane weight in gram, de is the isopropanol density in (g/m^3) and dp is the PVDF polymer density in (g/m^3).

2.6.5. Membrane thickness

Electrospun membranes thickness was measured after the heat-press treatment using a digital micrometre (Mitutoyo 293 Series, IP65) with a precision of ±0.001 mm. The given data is an average value of six measurements.

2.6.6. Membrane Morphology

The morphologies of electrospun membranes were characterized by field emission scanning electron microscope (FE-SEM, S-7400, Hitachi, Japan). All samples area about (1 × 1 cm) were coated with Cr at approximately 5 nm thickness by using a sputter coating device (Quorum model Q150TS) to reduce the charging effect on membrane surface. Image J program was used to calculate average fibre diameter of 100 measurements of high magnifications SEM images.

2.6.7. Air gap membrane distillation (AGMD) test

Membranes fabricated by electrospinning technique were tested by custom-made AGMD set-up as it shown in Figure 4. An insulation feed tank with 20 litter maximum capacity and pre-set heating system which consist of a heater coil and a controller from CAL Controls under the trade name Autotune temperature controller was used. A Gear pump (Tuthill Pump Co.) was used to pump the feed water in close system from the main tank by using a stainless-steel pipe (outside dimeter 6.35 mm) to the membrane cell via a flow meter. The horizontal stainless steel membrane cell details are as follow: dimension of 14.5 × 9.5 × 5.5 cm (L × W × H), air gap of 8 mm, effective membrane area of 36.88 m^2 and a rectangular feed channel with dimension of 520 × 4 × 3.2 mm (L × W × H). Aluminium perforated plates with the dimension of 100 × 50 (L × W) cm were used as a support layer underneath the membrane which prevent membrane deformation. The Cooler system was designed for providing pre-set cold water to the membrane cell with flow rate of 8.5 l/m. Four T- type thermocouples from (TC Ltd) were connected with the PC through TC-08 thermocouple data logger supplied by Pico technology was situated around the membrane cell (two for feed line and two for cooling line). In addition, two pressure gauges as well as a balance (Precision Lab Balance) were used. Equation 3 and 4 were used to calculate the permeate flux and rejection. The lead concentration in the feed and

permeate was measured by using Microwave Plasma Atomic Emission Spectroscopy (MP-AES) model 4200 from Agilent technology with the wavelength 340.458 nm.

$$J(\frac{L}{m^2 .h}) = \frac{\Delta g}{A.t.\rho} \quad (3)$$

$$R\ (\%) = \frac{C_f - C_p}{C_f} \times 100 \quad (4)$$

Where: J, Δg, ρ, t, A, R, C_f, and C_p represent water flux, weight of permeate (g), permeate density (g/cm^2), duration time (h), membrane effective area (m^2), rejection, feed concentration (mg/l), and permeate concentration (mg/l) respectively.

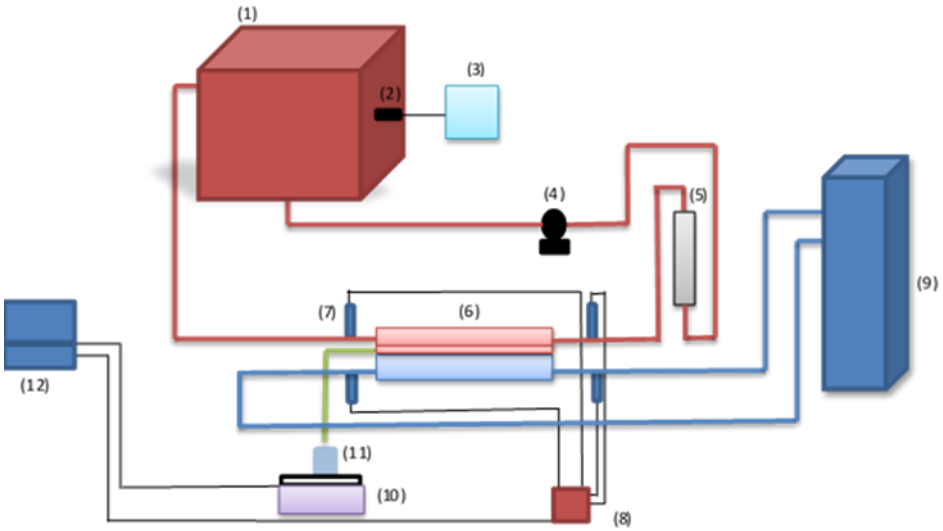

Figure 4: Schematic diagram of AGMD bench scale rig used in this study, (1) Feed Tank, (2) Heater, (3) Heater Controller, (4) Gear Pump, (5) Flowmeter, (6) Membrane Cell, (7) Thermocouple, (8) Thermocouple Data Logger, (9) Chiller, (10) Electronic Balance, (11) Beaker for permeate collection, (12) Computer.

3. Result and discussion

3.1. Membrane optimization

3.1.1. Effect of polymer concentration

Generally, Polymer solution concentration plays a crucial role in the membrane morphology as it controls solution viscosity and therefore effects both fibre diameter and beads formation. Three different polymer concentrations (15, 17.5, 20 wt%) were chosen with solvent mixture ratio DMF: Acetone (6:4). The electrospinning device parameters were as follow: polymer

flow rate 0.3 ml/h, three different values of high voltages (10, 14, 16 KV), distance between the needle and the drum 15 cm and actuator speed 8 cm/min. As can be seen from Figure 5, fibre diameters and standard deviation increase with the increase of polymer concentration, also the bead formation decreases due to boost of polymer viscosity with increasing polymer concentration. This is due to reduction of the breakup of the polymer chain by increasing of polymer viscosity [35]. These results are in agreement with Essalhi et al [36]. They showed that fibre diameter increased from 62.6 to 506.3 nm as well as fibre dimeter distribution became broader when the polymer viscosity varied from 0.364 to 9.380 Pa.s due to increase of PVDF concentration from 15 to 30 wt%. Furthermore, the same authors showed that the beads density reduced from 238.4 to 3.7 $\times 10^{-3}$ μm^{-2} by changing the polymer concertation from 15 to 22.5 wt%. Generally speaking, high surface tension and low polymer conductivity with insufficient molecular chain entanglements can cause an increase of beads numbers in electrospun mat due to the breakup of the polymer chain [35]. Figure 5d illustrates that fibre diameters decrease with increase of voltage supply, for instant, fibre diameter of 20 wt% polymer concentration decreases from 850 to 680 nm when the voltage increases from 10 to 16 KV. These results agree with Still et al. that showed reducing of fibre diameter with increasing of the electrical field in the needle tip is caused by strengthening of charge repulsion in the polymer solution and as a result stretch of the polymer solution [37].

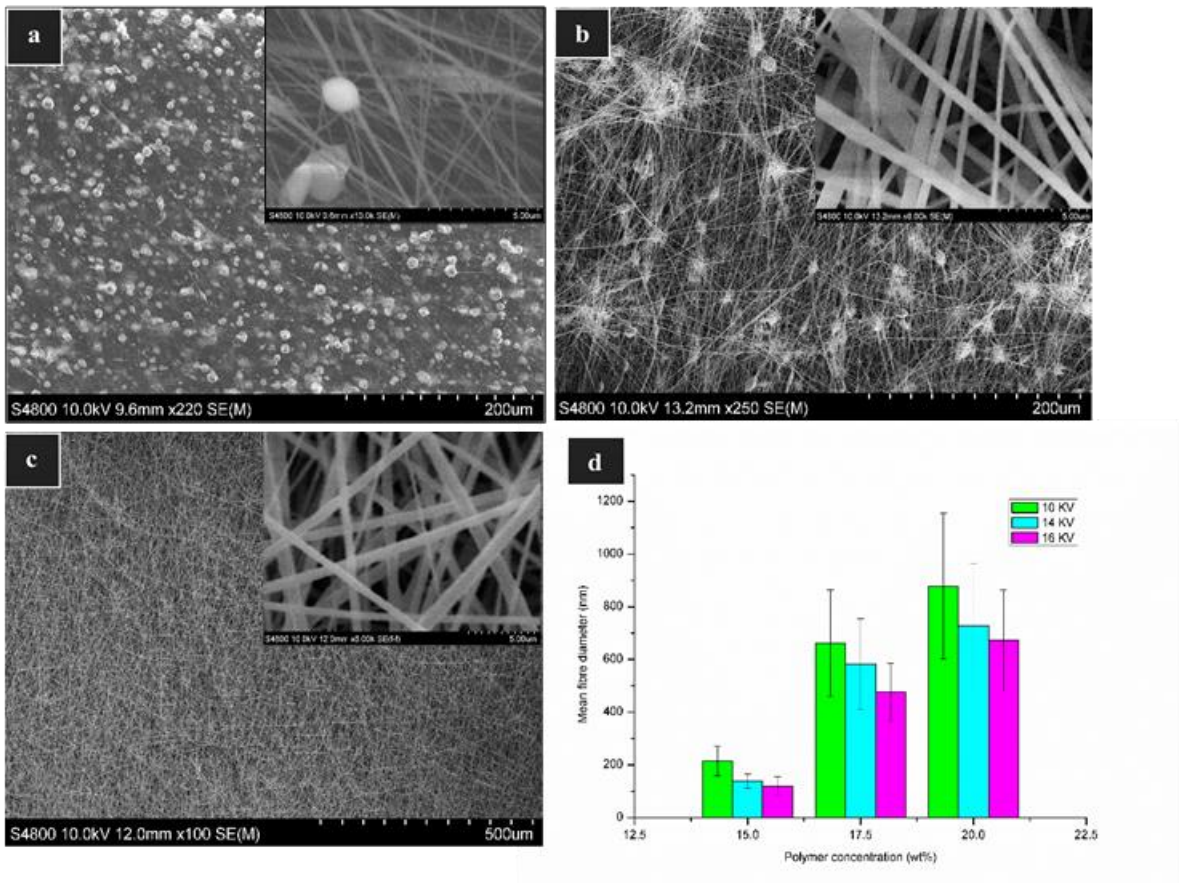

Figure 5: SEM images of fibres at various polymer concentrations, a) 15wt% PVDF, b) 17.5 wt% PVDF, c) 20 wt% PVDF, and d) effect of polymer concentration on the fibre diameters at various voltages.

3.1.2. Effect of mix solvent ratio

Solvent properties such as volatility, vapour pressure, dielectric constant and surface tension play important roles in electrospinning process. The DMF solvent has an adequate polyelectrolyte behaviour with a dipolar aprotic solvent due to having a high dielectric constant (36.7 at 25 ºC) [38]. However, DMF has low vapour pressure and high boiling point (153 ºC) which can be difficult to gain dry membrane mat by using it alone with PVDF polymer. Therefore, acetone (AC) was employed with DMF to increase the mixture vapour pressure as well as reducing mixture boiling point. Four different ratios of solvent mixture of DMF and AC was investigated by utilizing 15 wt% of PVDF polymer. Figure 6 illustrates that both fibre diameter and standard deviation of membrane mat increases with the increase of the acetone ratio due to the rapid evaporation rate of the solvent in the polymer solution between the spinneret and the drum. The number of beads is also diminished. In addition, 60:40 DMF:AC is seemed to be the best ratio to obtain small fibre diameter and dry membrane mat with less bead compared with 75:25 DMF: AC ratio. The SEM images in Figure 6 also show that beads formation decreases with the increase of acetone ratio. These results are in agreement with the

results accomplished by Zhou et al [39] in which beads reduced by increasing DMF to Acetone ratio in 12 wt% PVDF solution due to reduction in evaporation rate of the solvent mixture. Fibre diameter also reduced from 1710 to 410 nm by increasing the volume ratio of DMF/Acetone from 2:8 to 6:4.

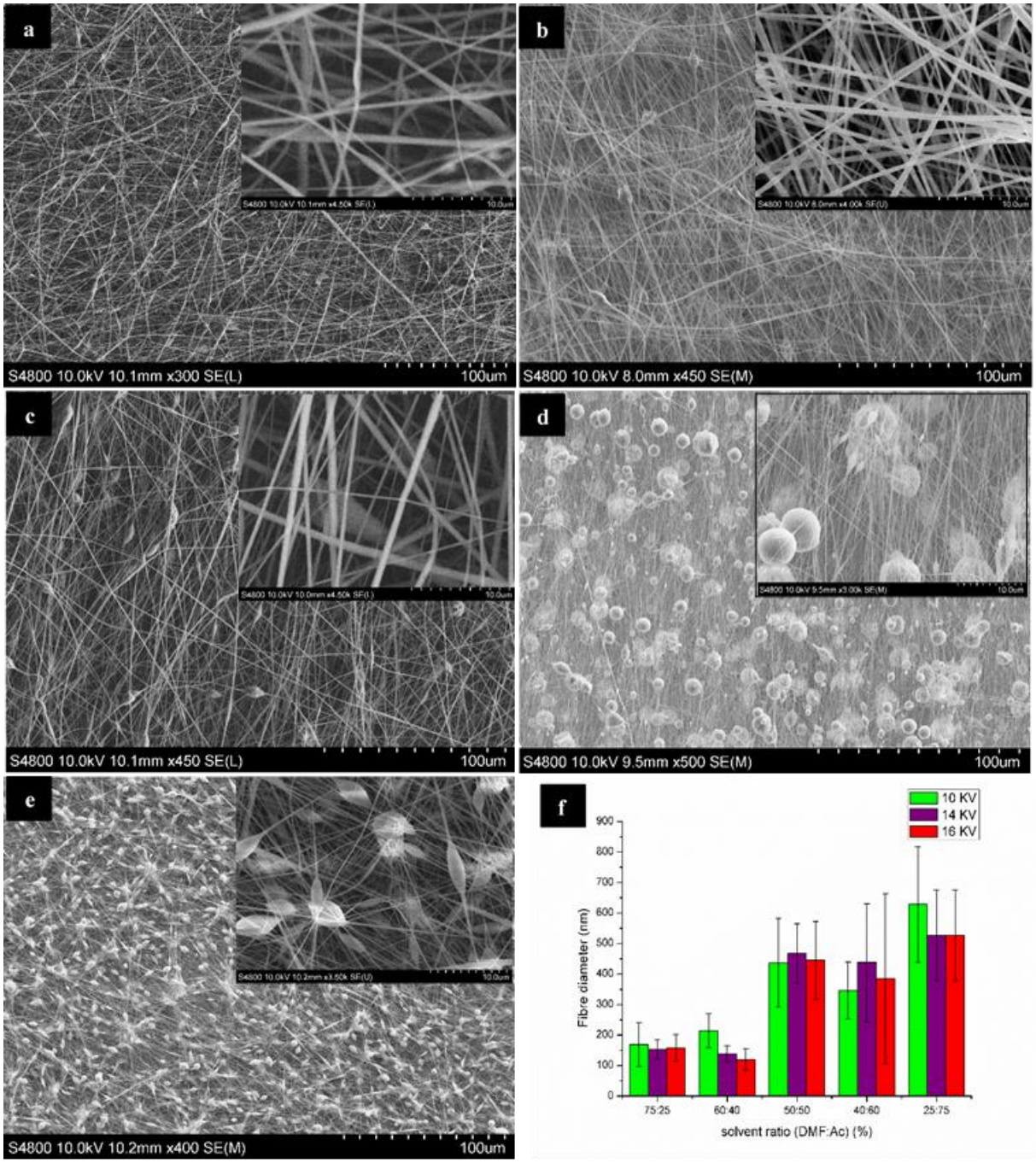

Figure 6: SEM images of fibres at various solvent ratios, a) 25% DMF, b) 40% DMF, c) 50% DMF, d) 60% DMF, e) 75% DMF, and f) the relation between fibre diameter and solvent ratio (DMF:AC).

3.1.3. Effect of surfactant addition on fibre formation

This section examines both average fibre dimeter and beads defect structures in membrane mat by adding a cationic surfactant (HTAB) to the PVDF polymer solution. Due to low electrical conductivity of the unmodified PVDF polymer solution, which is around 3 µS/cm, the chance of beads formation is very high. Tackling this issue can be achieved either by adding salt to increase solution conductivity or by adding a surfactant to reduce solution surface tension [40]. Two different concentrations of HTAB based on polymer weight were added to the PVDF solution. The electrospinning set up parameters were as follow: polymer flow rate between 0.2 to 0.4 ml/h, drum rotation speed 500 rpm and actuator speed 8 cm/min. Figure 7 shows the effect of adding 0, 0.05, 0.5 wt% of HTAB surfactant on fibre diameters at 14 KV Voltage. As it can be seen from the images and taking into account the standard deviation, there is not such a large deference on the average fibre diameter by adding 0.05 and 0.5 wt% HTAB. Figure 7b shows very uniform fibres without the presence of beads due to the presence of 0.05 wt% HTAB. The absence of beads is also clear at 0.5 wt% HTAB additions; however, the fibres are not as uniform in size compared to the fibres with 0.05 wt% HTAB. Based on the results, 0.05 wt% HTAB was used for further membrane studies. These results are in agreement with Zheng et al [41] in term of reduction of beads by adding HTAB surfactant to PVDF polymer solution and increase of fibre diameter, however, it was shown that the increase in fibre size distribution is not consistent with increase of HTAB concentration.

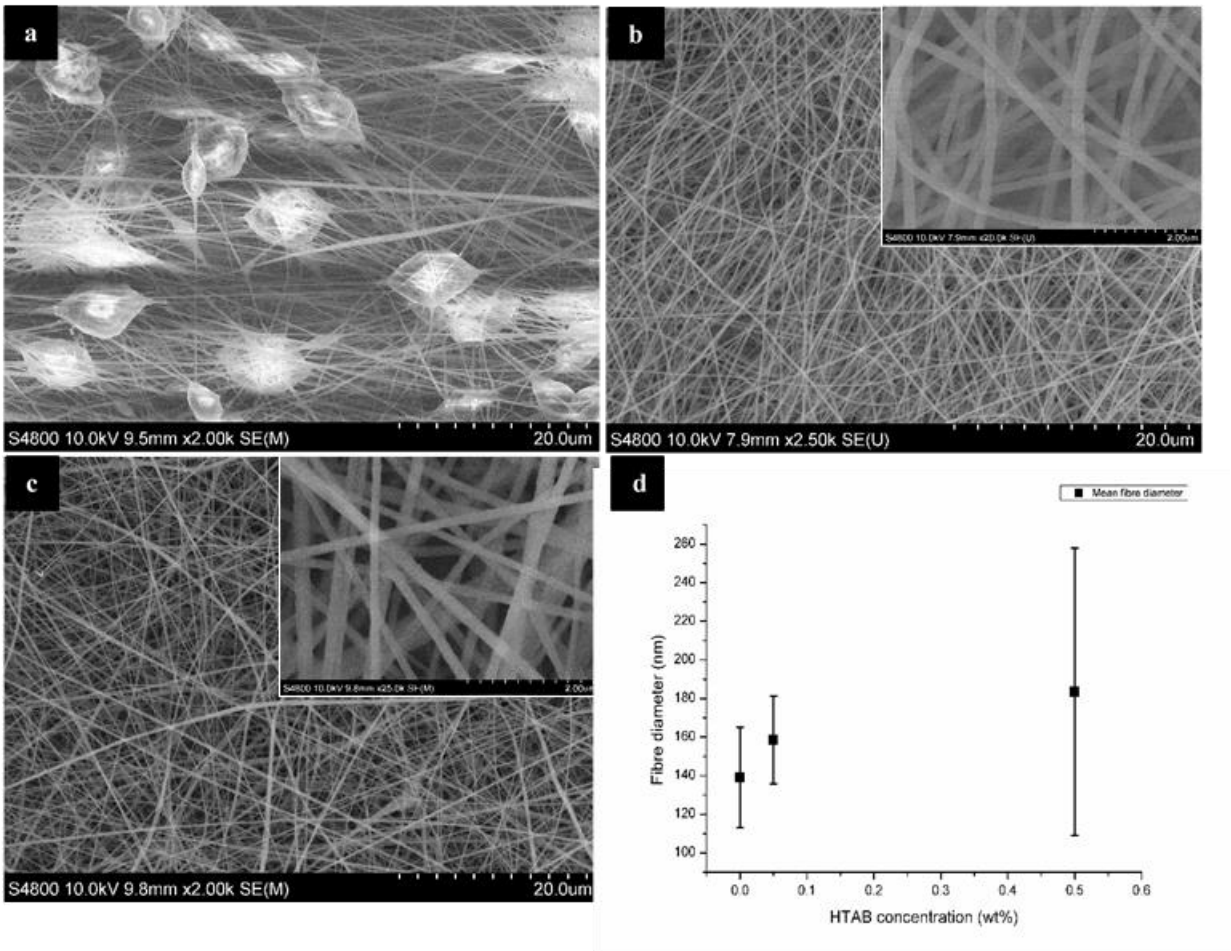

Figure 7, SEM images of fibres in the presence of HTAB, a: 15 wt% PVDF+ 0 wt% HTAB, b:15 wt% PVDF+0.05 HTAB, c: 15 wt% PVDF+0.5 HTAB, and d: the relation between fibre diameter and HTAB concentration.

3.2. Membrane characterization

3.2.1. Effect of Al_2O_3 addition on membrane structure

Based on the optimum PVDF concentration in section 4.1, PVDF with 15 wt% concentration and 0.05 wt% HTAB were used to examine the effect of superhydrophobic nanoparticles on the membrane structure. However, addition of Al_2O_3 NPs affected the polymer viscosity, and as a result lower concentration of PVDF (11, 13 wt%) were also considered. Figure 8 compares the morphological structures of composite PVDF ES membranes with three polymer concentrations and different concentrations of Al_2O_3 NPs. It can be observed that the average fibre diameters of the native membrane (with 15 wt% PVDF) increases slightly from 200 nm to 214 , 227, 236 and 272 nm with increasing the NPs concentration to 5, 10, 20, 30 wt%, respectively. While in the case of reducing the polymer concentration from 13 to 11 wt% PDVF in the presence of 20 wt% NPs, the fibres diameters decreased from 194.67 nm to 105 nm, respectively. This can be attributed to change of solution viscosity which is agreed with other

researchers [42, 43]. The results also show that alumina NPs can affected the distribution of fibre diameters as can be seen in Figure 8: PVDF fibres (15 wt%) with 5 and 10 wt% NPs have narrower size distribution compared to 20 and 30 wt% NPs. This might be due to the poorer dispersibility and agglomeration of alumina NPs at higher concentrations in the polymer solution and that leads to the irregular morphology of fibres in the final membrane.

Additionally, the effect of adding HTAB surfactant on hydrophobicity of functionalized alumina NPs was examined by measuring the contact angle of glass slides were spayed by 10 wt% of functionalised NPs in isopropanol with and without adding 0.05 wt% HTAB. The result showed that the contact angle was 153^0 for both samples which indicated that adding HTAB surfactant has no effect on NPs hydrophobicity.

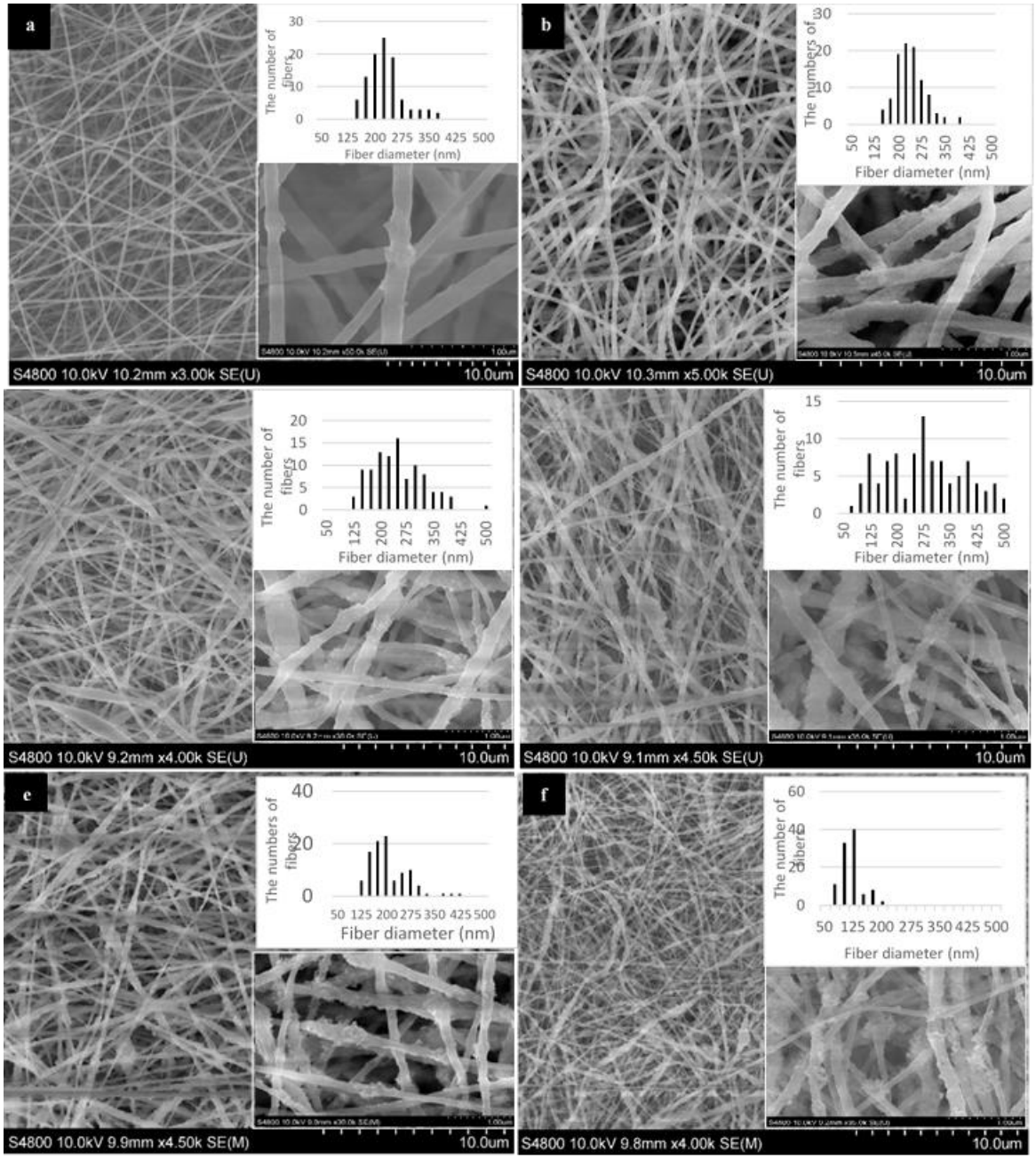

Figure 8: SEM images of fibres in the presence of Al_2O_3 NPs, a: 15 wt% PVDF with 5 wt% Al_2O_3, b: 15 wt% PVDF with 10 wt% Al_2O_3, c: 15 wt% PVDF with 20 wt% Al_2O_3, d: 15 wt% PVDF with 30 wt% Al_2O_3, e: 13 wt% PVDF with 20 wt% Al_2O_3, and f:11 wt% PVDF with 20 wt% Al_2O_3.

3.2.2. Membrane wetting properties

Membrane wettability relies on the roughness and the surface energy of membrane surface [44]. The effect on membrane hydrophobicity was investigated by adding different concentrations of modified alumina NPs (diameter =13 nm) with Isostearyl acids. It was shown previously that surface roughness is not the only factor in tuning surface wettability, and chemical functionality is also necessary in combination with roughness for superhydrophobicity as well as superhydrophilicity [29]. As a result and based on the WCA

and roughness data of the neat alumina NPs, it was decided to only examine the functionalized superhydrophobic nanoparticles in this work.

The WCA measurements along with full characterization of the three various PVDF concentrations with and without Al_2O_3 NPs are presented in Table 3. The pristine 15 wt% PVDF ES membrane showed a WCA of 132º. However, upon addition of 5, 10, 20, and 30 wt% of Al_2O_3 NPs to 15 wt% PVDF, the WCA increased to 139º, 140º, 141º, and 142º, respectively, which is higher than the neat 15 wt% PVDF (ES15-0). The increase of WCA of the membrane surface is due to an increase in the surface roughness and a decrease in the surface energy of the nanofiber due to the addition of superhydrophobic NPs. Interestingly, the value of WCA for 13 and 11 wt % of PVDF in the presence of 20 wt% Al_2O_3 NPs (ES13-20 and ES11-20) was increased to 145º and 150º respectively. Increasing the NPs ratio by reducing the polymer concentration contributed to an increase in the membrane roughness, as well as a formation of a fibre-bead structure on the membrane surface and a reduction of the fibre dimeter. Similar results were achieved in a electrospinning study when factionalized SiO_2 nanoparticle with n-dodecyltrimethoxysilane (DTMS) were mixed with polyurethane polymer [45].

3.2.3. Membrane pore size distribution (PSD), liquid entry pressure (LEP) and porosity

One of the factors that affects membrane quality in terms of water permeability and retention rate is the pore size and pore size distribution. Thus, the ES membrane pore size and maximum pore size characterization was carried out by a custom-made device represented by a bubble-point method. It can be seen from Table 3 that the membrane mean pore size increased from 0.47 to 0.715 µm by adding 20 wt% of alumina NPs to 15 wt% PVDF due to an increase in membrane fibre diameter. While, the mean pore size reduced from 0.47 to 0.37 µm by a reduction in polymer concentration from 15 to 11 wt% as a result of a decrease in mean fibre diameter from 200 to 105.74 nm.

Table 3 shows the LEP values of the neat and composite ES PVDF membranes. The value of LEP of PVDF 15 wt% was dropped from 17.11 to 14.22 psi by adding 20 wt% of alumina NPs. This is might be due to an increase in pore size from 0.47 to 0.715 µm. On the other hand, the LEP increased from 17.11 to 27 psi by reducing the polymer concentration from 15 to 11 wt%. This increase can be attributed to a reduction of mean pore size as well as an increase in membrane hydrophobicity with WCA of 132 (for ES15-0) and 150 º (for ES11-20).

The porosity of neat and composite membrane for 15 wt% PVDF concentration have shown a reduction pattern by adding alumina nanoparticles. Table 3 illustrates that by adding 20 wt% of alumina NPs, the porosity of ES15 membrane decreases by 8.8 percent due to the growth of nanofiber dimeter and accumulated of NPs on the fibres surface. Similar behaviour was observed by using 8 wt% of SiO_2 NPs incorporated with PVDF polymer which led to reduction of porosity by 6.8 % [46]. However, reducing the polymer concentration to 11 wt% and preserving the same amount of NPs lead to increase of membrane porosity to 0.912 %. This can be attributed to reduction of fibres diameter to 105.7 nm.

Table 3: Characterization values of commercial and fabricated membranes.

Membrane code	**Material**	**WCA, °**	**LEP, psi**	**Pore size, µm**			**Membrane thickness, µm**	**Porosity/%**	**Mean fibre diameter/ nm**
				mean	min	max			
ES15-0	15 wt% PVDF pristine	132	17.11	0.470	0.40	0.63	95 ± 2	0.895	200
ES15-20	15 wt% PVDF + 20 wt% Al_2O_3	141	14.22	0.715	0.528	0.90	110 ± 3	0.816	236.0
ES13-20	13 wt% PVDF + 20 wt% Al_2O_3	145	18.12	0.462	0.389	0.61	98 ± 2	0.872	194.67
ES11-20	11 wt% PVDF + 20 wt% Al_2O_3	150	27	0.370	0.322	0.467	100 ± 3	0.912	105.74
GVHP	GVHP 29325	123.8	30	0.220	-----	------	125 ± 2	0.75	-----

3.3. AGMD membrane performance

3.3.1. Flux pattern and permeate quality

The fabricated PVDF membrane performance was assessed by using AGMD in terms of the water permeability and heavy metal (Pb) rejection. Figure 9 shows the flux performance and percent of rejection of an aqueous solution with 1000 mg/l lead concentration over a period of 5 hours by implementing one commercial membrane and four fabricated membrane: The Commercial PVDF membrane under the trade name GVHP 29325 and four PVDF ES membranes (ES15-0, ES15-20, ES13-20 and ES11-20).

Figure 9a shows that the commercial PVDF membrane exhibited the lowest flux of around 15 LMH. On the other hand, high fluxes between 16.5 and 20 LMH have been shown by the neat and the composite PVDF membranes with Al_2O_3 NPs. This is higher than the PVDF electrospun membrane (11.8 LMH) which was fabricated by Feng et al by using 1000 mg/l NaCl at 60ºC as feed temperature [47]. The neat PVDF showed second highest flux around 19 LMH and this might be due to the fact that it has the second highest porosity after ES11-20 with good interconnected porous structure which plays a major role in increasing the membrane flux despite having a small mean pore size of 0.47 µm. In contrast, the 15 wt% PVDF with 20 wt% Al_2O_3 (ES15-20) showed a lower flux compared to the neat membrane (ES15-0) which is around 16.5 LMH despite having a larger mean pore size. This can be due to a lower porosity (0.816) and poorer inner connected pore structure in the membrane arrangement. Moreover, ES13-20 showed the water flux of about 18 LMH. The elevation of permeation flux compare to ES15-20 is due to increase in the membrane porosity despite the reduction of membrane mean pore size to 0.462 µm. ES11-20 exhibited the largest water flux nearly to 20 LMH and this is due to having the highest membrane porosity (0.912), the largest WCA (150º) and the highest LEP (almost 27 psi) which prevent the membrane from wetting.

Figure 9b shows the rejection percentage of Pb as a function of time. As can be observed from the data, neat PVDF (ES15-0) has the lowest rejection % and the rejection of lead was dropped from 84.2 to 72.7% within the five-hour operation despite having a high flux rate. This is due to the lower hydrophobicity properties of the neat PVDF membranes (WCA = 132º) and a smooth fibre surface which leads to the rapid membrane wetting. However, the modified membrane with 20 wt% alumina (ES15-20) showed an improved rejection rate of 92.5 % to 84 % within 5 hours. The increase in the rejection percentage by adding 20 wt% of NPs is due to an improved in the hydrophobicity of the membrane by 10º compared to the neat PVDF. The best result of rejection and a stable performance was achieved by membrane ES11-20 which showed over 99 % metal rejection within 5 hours. This is because of the highly hydrophobic properties of the membrane due to the presence of the superhydrophobic NPs, and the highest properties (WCA=150º , LEP= 27 psi).

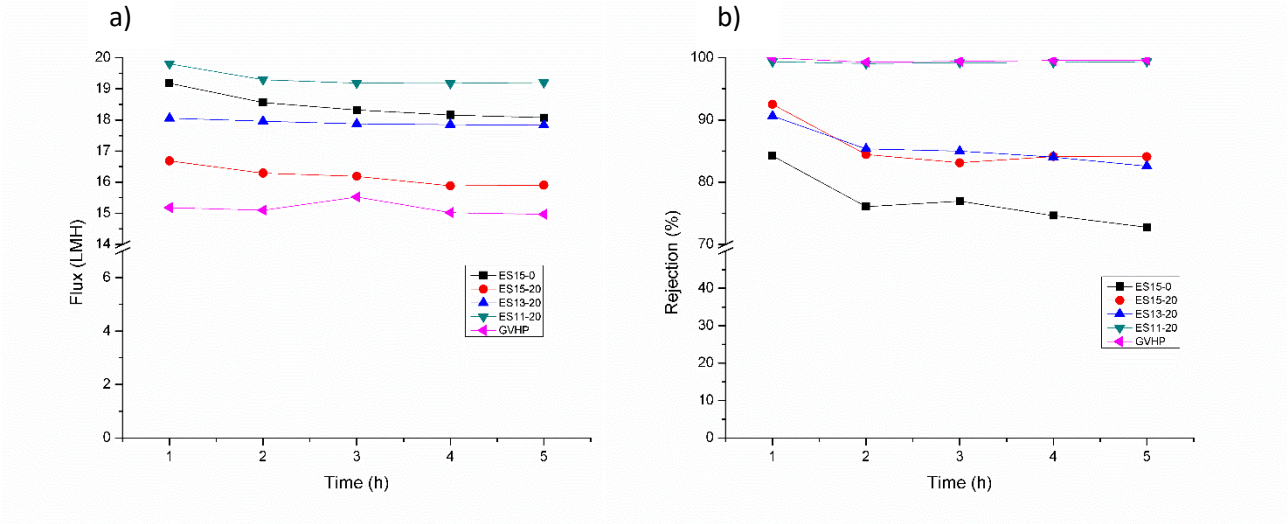

Figure 9: a) Flux data and b) rejection percentage as a function of time for the commercial and the synthesized membranes.

3.3.2. Effect of Pb concentration

Four different concentrations of Pb were chosen in order to study the effect of heavy metal concentration on both permeate flux and heavy metal rejection. Figure 10 illustrates the effect of four Pb concentrations (500, 1000, 1500, 2000 mg/l) by using the 11 wt% PVDF with 20 wt% NPs (ES11-20) membrane. As it was expected, the increase of lead concentration led to a slightly lower permeate flux from around 20 LMH to around 19 LMH (Figure 10a). This reduction could be attributed to decrease of the feed vapour pressure as well as the effect of temperature polarization by increase in the feed solution concentration as it was shown by other studies[48, 49]. Opposite trend was observed for the metal rejection % at which a small decrease in Pb rejection by about 0.8 % for the lowest concentration of lead. The high rejection % with high lead concentration can be attributed to high LEP (27 psi) of ES11-20 which results in high resistance to lead permeation at high concentration and this agreed with by Feng et al. [47] and Moradi [50].

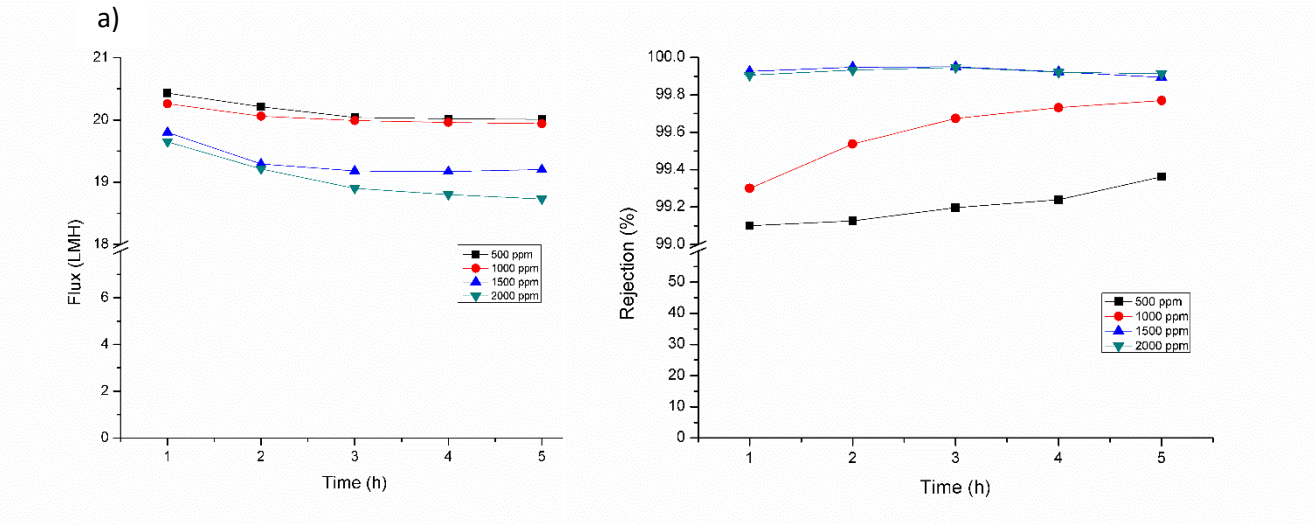

Figure 10: Measurement of a) flux rate vs time and b) rejection percentage vs time for various lead concentrations using ES11-20 membrane.

4. Conclusions

Highly hydrophobic nanofibrous PVDF membranes were successfully prepared using superhydrophic Al_2O_3 nanoparticles. Whereas prior work has shown that various superhydrophobic membranes can be prepared using nanoparticles functionalized by silane and fluorocarbons [25,26,31,32], this work demonstrates for the first time that superhydrophobic PVDF membranes can be prepared using branched hydrocarbon functionalized NPs.

In this paper, electrospinning solution parameters such as polymer concentration and solvent ratio, effect of HTAB surfactant and superhydrophobic alumina NPs addition was examined to fabricate highly hydrophobic nanofibrous PVDF membranes. The results showed that uniform hydrophobic nanofibrous membrane with beadless small fibres diameter can be achieved by using high voltage of 14-16 KV, drum to needle distance of 15 cm, PVDF polymer solution of 15 wt%, 6:4 ratio of DMF to acetone solvent, and 0.05 wt% of HTAB. Moreover, membrane hydrophobicity was improved by incorporating different concentrations of superhydrophobic Al_2O_3 NPs with PVDF polymer solution. The outcomes demonstrated that in the presence of alumina NPs less PVDF polymer concentration is needed. Also the membrane contact angle and its LEP was boosted and the membrane pore size was reduced. The superhydrophobic PVDF membrane was enhanced in AGMD to treat waste water with high concentration of lead. High rejection percentage and flux rate was fulfilled by using 11 wt% of PVDF concentration with 20 wt% of superhydrophobic NPs. It can be concluded that superhydrophobic alumina NPs functionalized with highly branched hydrocarbons can be used successfully to improve

MD membrane hydrophobicity and performance as well as in removing of toxic and hazardous inorganic pollutants.

ACKNOWLEDGMENT

The authors would like thank the Ministry of Higher Education and Scientific Research/Iraq and Al-Mustansiriya University/ Baghdad for providing PhD scholarship for Hadi Attia and acknowledge the Welsh Government for providing a Sêr Cymru II Welsh Fellowship which is part-funded by the European Regional Development Fund (ERDF) for Shirin Alexander.

References:

[1] E. Drioli, A. Ali, F. Macedonio, Membrane distillation: Recent developments and perspectives, Desalination, 356 (2015) 56-84.
[2] O.B. Akpor, G. Ohiobor, T. Olaolu, Heavy metal pollutants in wastewater effluents: sources, effects and remediation, Adv. Biosci. Bioeng, 2 (2014) 37-43.
[3] M. Barakat, New trends in removing heavy metals from industrial wastewater, Arabian Journal of Chemistry, 4 (2011) 361-377.
[4] S. Khaoya, U. Pancharoen, Removal of lead (II) from battery industry wastewater by HFSLM, International Journal of Chemical Engineering and Applications, 3 (2012) 98.
[5] M. Arbabi, S. Hemati, M. Amiri, Removal of lead ions from industrial wastewater: A review of Removal methods, International Journal of Epidemiologic Research, 2 (2015) 105-109.
[6] S. Gunatilake, Methods of Removing Heavy Metals from Industrial Wastewater, Methods, 1 (2015).
[7] F. Fu, Q. Wang, Removal of heavy metal ions from wastewaters: a review, J Environ Manage, 92 (2011) 407-418.
[8] J.A. Pandya, Nanofiltration for Recovery of Heavy Metal from Waste Water.
[9] M.A. Barakat, New trends in removing heavy metals from industrial wastewater, Arabian Journal of Chemistry, 4 (2011) 361-377.
[10] K. Košutić, L. Furač, L. Sipos, B. Kunst, Removal of arsenic and pesticides from drinking water by nanofiltration membranes, Separation and Purification Technology, 42 (2005) 137-144.
[11] F. Fu, Q. Wang, Removal of heavy metal ions from wastewaters: a review, Journal of environmental management, 92 (2011) 407-418.
[12] M. Zhao, Y. Xu, C. Zhang, H. Rong, G. Zeng, New trends in removing heavy metals from wastewater, Applied microbiology and biotechnology, 100 (2016) 6509-6518.
[13] Y. Liao, Design and fabrication of superhydrophobic membranes by electrospinning for direct contact membrane distillation, in: IDA Journal of Desalination and Water Reuse, 2014, pp. 154-154.
[14] A. Alklaibi, N. Lior, Comparative study of direct-contact and air-gap membrane distillation processes, Ind Eng Chem Res, 46 (2007) 584-590.
[15] B.L. Pangarkar, M. Sane, Performance of air gap membrane distillation for desalination of ground water and seawater, World Academy of Science, Engineering, and Technology, 75 (2011).
[16] A. Alkhudhiri, N. Darwish, N. Hilal, Membrane distillation: A comprehensive review, Desalination, 287 (2012) 2-18.

[17] Y.C. Woo, Y. Kim, W.-G. Shim, L.D. Tijing, M. Yao, L.D. Nghiem, J.-S. Choi, S.-H. Kim, H.K. Shon, Graphene/PVDF flat-sheet membrane for the treatment of RO brine from coal seam gas produced water by air gap membrane distillation, Journal of Membrane Science, 513 (2016) 74-84.
[18] P.P. Zolotarev, V.V. Ugrozov, I.B. Volkina, V.M. Nikulin, Treatment of waste water for removing heavy metals by membrane distillation, Journal of Hazardous Materials, 37 (1994) 77-82.
[19] A.M. Islam, Membrane distillation process for pure water and removal of arsenic, in, Chalmers University of Technology, Gothenburg, Sweden, 2004.
[20] F. Macedonio, E. Drioli, Pressure-driven membrane operations and membrane distillation technology integration for water purification, Desalination, 223 (2008) 396-409.
[21] P. Pal, A.K. Manna, Removal of arsenic from contaminated groundwater by solar-driven membrane distillation using three different commercial membranes, Water Res, 44 (2010) 5750-5760.
[22] R. Moradi, S.M. Monfared, Y. Amini, A. Dastbaz, Vacuum enhanced membrane distillation for trace contaminant removal of heavy metals from water by electrospun PVDF/TiO2 hybrid membranes, Korean Journal of Chemical Engineering, 33 (2016) 2160-2168.
[23] J. Prince, G. Singh, D. Rana, T. Matsuura, V. Anbharasi, T. Shanmugasundaram, Preparation and characterization of highly hydrophobic poly (vinylidene fluoride)–Clay nanocomposite nanofiber membranes (PVDF–clay NNMs) for desalination using direct contact membrane distillation, Journal of Membrane Science, 397 (2012) 80-86.
[24] L.D. Tijing, Y.C. Woo, W.-G. Shim, T. He, J.-S. Choi, S.-H. Kim, H.K. Shon, Superhydrophobic nanofiber membrane containing carbon nanotubes for high-performance direct contact membrane distillation, Journal of Membrane Science, 502 (2016) 158-170.
[25] X.Y. Xiong Li, Cheng Cheng, Li Deng, Min Wang, and Xuefen Wang, Electrospun Superhydrophobic Organic/Inorganic Composite Nanofibrous Membranes for Membrane Distillation, Applied Materials and Interfaces, (2015).
[26] E.-J. Lee, A.K. An, H. Pejman, S. Lee, Y.C. Woo, H.K. Shon, Advanced multi-nozzle electrospun functionalized titanium dioxide/polyvinylidene fluoride-co-hexafluoropropylene (TiO 2/PVDF-HFP) composite membranes for direct contact membrane distillation, Journal of Membrane Science, (2016).
[27] M. Sagisaka, T. Narumi, M. Niwase, S. Narita, A. Ohata, C. James, A. Yoshizawa, E. Taffin de Givenchy, F. Guittard, S. Alexander, J. Eastoe, Hyperbranched hydrocarbon surfactants give fluorocarbon-like low surface energies, Langmuir, 30 (2014) 6057-6063.
[28] S. Alexander, J. Eastoe, A.M. Lord, F.d.r. Guittard, A.R. Barron, Branched hydrocarbon low surface energy materials for superhydrophobic nanoparticle derived surfaces, Acs Appl Mater Inter, 8 (2015) 660-666.
[29] W. Al-Shatty, A.M. Lord, S. Alexander, A.R. Barron, Tunable Surface Properties of Aluminum Oxide Nanoparticles from Highly Hydrophobic to Highly Hydrophilic, ACS Omega, 2 (2017) 2507-2514.
[30] D. Qu, J. Wang, D. Hou, Z. Luan, B. Fan, C. Zhao, Experimental study of arsenic removal by direct contact membrane distillation, J Hazard Mater, 163 (2009) 874-879.
[31] A. Boubakri, R. Bouchrit, A. Hafiane, S.A.-T. Bouguecha, Fluoride removal from aqueous solution by direct contact membrane distillation: theoretical and experimental studies, Environmental Science and Pollution Research, 21 (2014) 10493-10501.
[32] T. Ogawa, B. Ding, Y. Sone, S. Shiratori, Super-hydrophobic surfaces of layer-by-layer structured film-coated electrospun nanofibrous membranes, Nanotechnology, 18 (2007) 165607.

[33] Y. Liao, C.H. Loh, R. Wang, A.G. Fane, Electrospun superhydrophobic membranes with unique structures for membrane distillation, ACS Appl Mater Interfaces, 6 (2014) 16035-16048.
[34] L.D. Tijing, Y.C. Woo, M.A.H. Johir, J.-S. Choi, H.K. Shon, A novel dual-layer bicomponent electrospun nanofibrous membrane for desalination by direct contact membrane distillation, Chem Eng J, 256 (2014) 155-159.
[35] S. Haider, Y. Al-Zeghayer, F.A. Ahmed Ali, A. Haider, A. Mahmood, W.A. Al-Masry, M. Imran, M.O. Aijaz, Highly aligned narrow diameter chitosan electrospun nanofibers, J Polym Res, 20 (2013).
[36] M. Essalhi, M. Khayet, Self-sustained webs of polyvinylidene fluoride electrospun nano-fibers: Effects of polymer concentration and desalination by direct contact membrane distillation, Journal of Membrane Science, 454 (2014) 133-143.
[37] T.J. Sill, H.A. von Recum, Electrospinning: applications in drug delivery and tissue engineering, Biomaterials, 29 (2008) 1989-2006.
[38] M.K. Souhaimi, T. Matsuura, Membrane distillation: principles and applications, Elsevier, 2011.
[39] Y. Zhou, L.R. Yao, Q. Gao, Preparation of PVDF nanofibrous membrane and its waterproof and breathable property, in: Advanced Materials Research, Trans Tech Publ, 2013, pp. 327-330.
[40] K. Nartetamrongsutt, G.G. Chase, The influence of salt and solvent concentrations on electrospun polyvinylpyrrolidone fiber diameters and bead formation, Polymer, 54 (2013) 2166-2173.
[41] J.-Y. Zheng, M.-F. Zhuang, Z.-J. Yu, G.-F. Zheng, Y. Zhao, H. Wang, D.-H. Sun, The effect of surfactants on the diameter and morphology of electrospun ultrafine nanofiber, Journal of Nanomaterials, 2014 (2014) 8.
[42] A.K. An, E.-J. Lee, J. Guo, S. Jeong, J.-G. Lee, N. Ghaffour, Enhanced vapor transport in membrane distillation via functionalized carbon nanotubes anchored into electrospun nanofibres, Sci Rep-Uk, 7 (2017) 41562.
[43] S. Huang, L. Zhou, M.-C. Li, Q. Wu, Y. Kojima, D. Zhou, Preparation and properties of electrospun poly (vinyl pyrrolidone)/cellulose nanocrystal/silver nanoparticle composite fibers, Materials, 9 (2016) 523.
[44] G. McHale, N. Shirtcliffe, M. Newton, Super-hydrophobic and super-wetting surfaces: analytical potential?, Analyst, 129 (2004) 284-287.
[45] S. Jin, Y. Park, C.H. Park, Preparation of breathable and superhydrophobic polyurethane electrospun webs with silica nanoparticles, Text Res J, 86 (2016) 1816-1827.
[46] Z.-Q. Dong, X.-H. Ma, Z.-L. Xu, Z.-Y. Gu, Superhydrophobic modification of PVDF–SiO2electrospun nanofiber membranes for vacuum membrane distillation, RSC Adv., 5 (2015) 67962-67970.
[47] C. Feng, K. Khulbe, T. Matsuura, R. Gopal, S. Kaur, S. Ramakrishna, M. Khayet, Production of drinking water from saline water by air-gap membrane distillation using polyvinylidene fluoride nanofiber membrane, Journal of Membrane Science, 311 (2008) 1-6.
[48] A.E. Khalifa, S.M. Alawad, M.A. Antar, Parallel and series multistage air gap membrane distillation, Desalination, 417 (2017) 69-76.
[49] J. Xu, Y.B. Singh, G.L. Amy, N. Ghaffour, Effect of operating parameters and membrane characteristics on air gap membrane distillation performance for the treatment of highly saline water, Journal of Membrane Science, 512 (2016) 73-82.
[50] R. Moradi, J. Karimi-Sabet, M. Shariaty-niassar, Y. Amini, Experimental investigation of nanofibrous poly (vinylidene fluoride) membranes for desalination through air gap membrane distillation process, Korean Journal of Chemical Engineering, 33 (2016) 2953-2960.